

Variation of galactic cold gas reservoirs with stellar mass

Natasha Maddox^{*1,2}, Kelley M. Hess^{1,3,2}, Danail Obreschkow⁴, M. J. Jarvis^{5,6}, S.-L. Blyth¹

¹*Astrophysics, Cosmology and Gravity Centre (ACGC), Astronomy Department, University of Cape Town, Private Bag X3, 7701 Rondebosch, Republic of South Africa*

²*Netherlands Institute for Radio Astronomy (ASTRON), PO Box 2, 7990 AA Dwingeloo, The Netherlands*

³*Kapteyn Astronomical Institute, University of Groningen, PO Box 800, 9700 AV Groningen, The Netherlands*

⁴*International Centre for Radio Astronomy Research (ICRAR), M468, University of Western Australia, 35 Stirling Hwy, Crawley, WA 6009, Australia*

⁵*Oxford Astrophysics, Denys Wilkinson Building, University of Oxford, Keble Rd, Oxford, OX1 3RH, UK*

⁶*Physics Department, University of the Western Cape, Cape Town, 7535, Republic of South Africa*

10 September 2018

ABSTRACT

The stellar and neutral hydrogen (HI) mass functions at $z \sim 0$ are fundamental benchmarks for current models of galaxy evolution. A natural extension of these benchmarks is the two-dimensional distribution of galaxies in the plane spanned by stellar and HI mass, which provides a more stringent test of simulations, as it requires the HI to be located in galaxies of the correct stellar mass. Combining HI data from the ALFALFA survey, with optical data from SDSS, we find a distinct envelope in the HI-to-stellar mass distribution, corresponding to an upper limit in the HI fraction that varies monotonically over five orders of magnitude in stellar mass. This upper envelope in HI fraction does not favour the existence of a significant population of dark galaxies with large amounts of gas but no corresponding stellar population. The envelope shows a break at a stellar mass of $\sim 10^9 M_{\odot}$, which is not reproduced by modern models of galaxy populations tracing both stellar and gas masses. The discrepancy between observations and models suggests a mass dependence in gas storage and consumption missing in current galaxy evolution prescriptions. The break coincides with the transition from galaxies with predominantly irregular morphology at low masses to regular disks at high masses, as well as the transition from cold to hot accretion of gas in simulations.

Key words: surveys–galaxies:general–galaxies:evolution–galaxies:stellar content–radio lines:galaxies

1 INTRODUCTION

Despite the great advances that have been made, understanding how galaxies form and evolve with time remains an ongoing challenge in modern astronomy. Galaxies are complex, with the relevant physics occurring on size scales ranging from individual stars and black holes through to galaxy clusters. A multi-wavelength approach to the problem is clearly required, as the different processes and evolutionary stages are characterised by emission mechanisms spanning the full electromagnetic spectrum.

Although observations of the stellar component of

galaxies are routinely made for large samples of objects over significant sky areas (e.g. Sloan Digital Sky Survey, SDSS, York et al. 2000) to high redshift (e.g. VIMOS VLT Deep Survey, VVDS, Le Fèvre et al. 2005), observations of the gas in galaxies lags behind. As cold gas serves as the reservoir from which stars form, the non-trivial relationship between the gas and stellar content of galaxies is fundamental to understanding their evolution. Observations of both the stellar and gaseous components of galaxies are required to illuminate the interplay between the two.

Targeted observations of small numbers of individual galaxies provide important insight. The HI Nearby Galaxy Survey (THINGS, Walter et al. 2008) focuses on relatively local, highly resolved galaxies, enabling discrete sites of star

* maddox@astron.nl

formation activity to be individually assessed based on observations of the neutral and molecular gas (Bigiel et al. 2008). From these specific studies, the general relations, observed on galaxy scales, can be better understood (such as the Kennicutt-Schmidt law for star formation; Kennicutt 1998, or Bigiel & Blitz 2012).

Large surveys, although insensitive to the details extracted from targeted observations, reveal global trends governing the general population. Often, statistical studies of such surveys provide insight into processes too subtle to discern from individual objects. At optical wavelengths, the SDSS has been particularly effective at uncovering global trends in the stellar properties of galaxies, such as the red sequence and blue cloud galaxy bimodality seen by Baldry et al. (2004), for example.

The Square Kilometre Array (SKA, Carilli & Rawlings 2004) will revolutionize the study of extragalactic gas reservoirs, enabling neutral hydrogen (HI) to be observed to $z \sim 1$ over a significant fraction of the sky, bringing HI observations more in line with optical surveys, both in terms of sensitivity and area coverage. The SKA pathfinder and precursor instruments APERTIF (Verheijen et al. 2008), MeerKAT (Jonas 2009) and the Australian Square Kilometre Array Pathfinder (ASKAP, Johnston et al. 2008), currently under construction will already represent great advances themselves, due to innovative receiver design and expanded frequency range.

Along with advancing instrumentation, models of galaxy evolution are becoming increasingly sophisticated, with improved mass resolution and more physical prescriptions. In modern semi-analytic models, galaxy baryonic mass is partitioned into gas and stars, while the gas is further subdivided into atomic and molecular components using a variety of methods (Obreschkow et al. 2009a, Lagos et al. 2011, Popping et al. 2012). The interplay between gas and stars is then governed by prescriptions based on local conditions. Smoothed particle hydrodynamic simulations, such as those of Davé et al. (2013), have the resolution required to follow the detailed dynamics of gas and stars on sub-galactic scales, but have insufficient volume to model statistically representative samples of galaxies. These simulations are invaluable, as they allow us to explore the interactions between the various galactic components, including the influence of the dark matter haloes (Popping, Somerville, & Trager 2014).

In the current work, we focus on the dependence of HI mass (M_{HI}) on stellar mass within the HI-selected galaxy population, and we exploit this framework to compare observations with simulations. The relation between the stellar and gaseous components in galaxies appears straightforward at first glance, but the details provide insight into the history of both gas accretion and star formation, and reveals the potential for further star formation. Differences between the observed and simulated relations offer the opportunity to explore missing physics or other factors driving galaxy evolution currently not incorporated in the simulations. The data we use are described in Section 2, and presented in Section 3. A discussion of the results and suggestions for further lines of investigation are in Section 4. Concordance cosmology with $H_0 = 70 \text{ km s}^{-1} \text{ Mpc}^{-1}$ (thus $h \equiv H_0/[100 \text{ km s}^{-1} \text{ Mpc}^{-1}] = 0.7$), $\Omega_m = 0.3$, $\Omega_\Lambda = 0.7$ is assumed when computing masses and luminosities.

2 HI AND OPTICAL DATA

The HI data for the current work come from the Arecibo Legacy Fast ALFA survey (ALFALFA, Giovanelli et al. 2005), specifically the $\alpha.40$ HI source catalogue from Haynes et al. (2011), which covers $\sim 2800 \text{ deg}^2$, or 40 per cent of the final survey area. ALFALFA is a flux-limited survey, with sufficient sensitivity to detect galaxies with $M_{\text{HI}} = 3 \times 10^7 M_\odot$ at the distance of the Virgo Cluster (corresponding to $\sim 0.47 \text{ Jy km s}^{-1}$), while the spectral range allows observations of galaxies to $z = 0.06$. HI profile widths, recession velocities, distances and HI masses are derived by the ALFALFA team for each of the 15 855 objects in the catalogue. Of these, 15 041 are confident HI detections (HI code 1 or 2 in the ALFALFA catalogue), with the remainder being primarily high velocity clouds, not at extragalactic distances.

The $\alpha.40$ catalogue has been carefully crossmatched to the SDSS Data Release 7 (DR7, Abazajian et al. 2009) by members of the ALFALFA team to identify the most likely optical counterparts for the HI detections. The cross-matched catalogues provide the SDSS objID and specObjID identifiers of the optical galaxies (see Haynes et al. 2011 for a full description of the catalogue). 11 740 of the 15 855 ALFALFA galaxies have confident HI detections and unambiguous, clean optical counterparts in the SDSS photometry (optical counterpart code I in the ALFALFA catalogue). We refer to this subset as the ALFALFA–SDSS sample. HI-detected galaxies lying outside the SDSS footprint (2312 objects) are the primary cause for ALFALFA galaxies having no optical counterpart.

A collaboration of researchers at the Max Planck Institute for Astrophysics (MPA) and the Johns Hopkins University (JHU) have produced a value-added galaxy catalogue (hereinafter referred to as the *MPA–JHU catalogue*), which provides additional metrics derived from an independent analysis of the SDSS DR7 galaxy photometry and spectra. Objects must have an SDSS spectrum to appear in the MPA–JHU catalogue. Details of the analyses can be found in Tremonti et al. (2004) and Brinchmann et al. (2004), or at the website hosting the catalogues¹. Of the ALFALFA–SDSS sample, 9471 have entries in the MPA–JHU catalogue.

From the MPA–JHU catalogue, we extract measures of the stellar masses (M_*), derived by fitting the five optical SDSS photometry bands with a grid of updated stellar population synthesis models based on Bruzual & Charlot (2003). The MPA–JHU group compared these masses with those from Kauffmann et al. (2003) derived from spectral features and found good agreement over all masses. At the low mass end, there is also good agreement between the MPA–JHU stellar masses and those computed from UV–optical photometry by Huang et al. (2012a) for the galaxies contained in both samples. Of the 9471 galaxies in the MPA–JHU catalogue, 9153 have reliable stellar mass estimates, which we refer to as the spectroscopic ALFALFA–SDSS sample, and use in the following sections.

We have chosen to use ALFALFA for the current study, instead of, for example, the HI Parkes All-Sky Survey (HIPASS, Barnes et al. 2001, Meyer et al. 2004) due to the

¹ <http://www.strw.leidenuniv.nl/~jarle/SDSS>

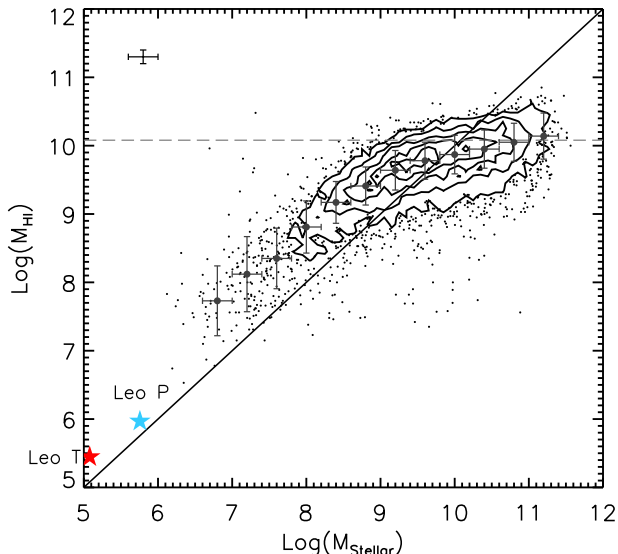


Figure 1. The relation between M_{HI} and M_* , in units of M_\odot , from the 9153 H I-selected ALFALFA galaxies with SDSS spectra and stellar masses from the MPA–JHU catalogue. The diagonal black solid line marks the 1-to-1 relation, while the horizontal grey dashed line indicates the approximate 50 per cent completeness limit for profiles of width 150 km s^{-1} at $z = 0.06$, the highest redshift probed. The dark grey points with error bars show the median and $1-\sigma$ values from the first three columns of Table 1. The blue and red stars denote the very low mass Leo P and Leo T dwarf galaxies. Typical uncertainties on M_{HI} and M_* are 10 and 20 per cent, respectively, indicated by the example point in the top left corner with error bars. The few points at low stellar mass and $M_{\text{HI}} > 10^9 M_\odot$ are pairs of galaxies within one ALFALFA beam at similar redshift, causing confusion with their H I profiles. The contour levels are at 5, 15, 30, 45, and 60 points computed on a grid with 0.1 intervals in $\log(M_{\text{HI}})$ and $\log(M_*)$.

corresponding availability of homogeneous, high quality ancillary photometry and spectroscopy from SDSS.

3 H I MASS VS STELLAR MASS

In Fig. 1, we show M_{HI} plotted as a function of M_* for the spectroscopic ALFALFA–SDSS galaxy sample, which spans more than five orders of magnitude in stellar mass, and nearly four orders of magnitude in H I mass. The diagonal black line marks the 1-to-1 relation of equal H I and stellar masses. The points show a clear correlation, with M_{HI} increasing as a function of M_* , and a break in the slope of the relation at $M_* \sim 10^9 M_\odot$. Similar plots, such as Figure 2a of Huang et al. (2012b), also show this behaviour. The median and $1-\sigma$ values for the data in Fig. 1 in bins of stellar mass are tabulated in Table 1.

It is known that more massive galaxies have higher molecular gas to neutral gas ratios ($\text{H}_2/\text{H I}$, Blitz & Rosolowsky 2006, Leroy et al. 2008). In order to maintain a continuous 1-to-1 relation from low to high masses, the mass of H_2 required at the high mass end is of the order of the mass of H I, and galaxies with such large amounts of molecular gas are not observed in the disk galaxies which dominate the ALFALFA sample.

Table 1. Median and $1-\sigma$ values for the data shown in Fig. 1 and Fig. 3. The first column lists the centre of the $\log(M_*)=0.4$ width bins. The second and third columns are derived only from galaxies with SDSS spectra, whereas the fourth and fifth columns include galaxies without a spectrum. Note that the width of the distribution of points is not symmetric about the median, thus the $1-\sigma$ values are provided only for guidance.

$\log(M_*)$ M_\odot	Median $\log(M_{\text{HI}})$ M_\odot	$1-\sigma$ M_\odot	Median $\log(M_{\text{HI}})$ M_\odot	$1-\sigma$ M_\odot
6.8	7.73	0.51	8.13	0.67
7.2	8.12	0.55	8.44	0.63
7.6	8.35	0.44	8.68	0.59
8.0	8.81	0.38	8.99	0.45
8.4	9.17	0.31	9.23	0.34
8.8	9.41	0.28	9.43	0.30
9.2	9.64	0.29	9.64	0.30
9.6	9.78	0.27	9.77	0.28
10.0	9.87	0.28	9.86	0.29
10.4	9.95	0.28	9.95	0.29
10.8	10.05	0.28	10.04	0.29
11.2	10.14	0.34	10.14	0.33

At the high stellar mass end, the galaxies’ H I content is weakly dependent on stellar mass. These galaxies are dominated by metal-enriched disks, with gas-phase oxygen metallicities, $12+\log(\text{O}/\text{H})$, compiled by the MPA–JHU group, reaching solar values and above. This is consistent with the conclusion reached in Huang et al. (2012b), which shows that the ALFALFA population primarily exists within the blue cloud. The number counts of H I-detected early-type and spiral galaxies within the ATLAS^{3D} project also show that disks dominate at large masses (Serra et al. 2012). At lower stellar masses, below the break at $M_* \sim 10^9 M_\odot$, the galaxies have relatively high H I fractions, are metal poor, and as discussed in Section 4.1.2, tend to have irregular morphology.

The blue star in the bottom left corner of Fig. 1 is the Leo P dwarf galaxy, while the red star at even lower mass is the Leo T dwarf galaxy, indicating that the linear relation between M_{HI} and M_* at $M_{\text{HI}} < 10^9 M_\odot$ appears to continue to very low neutral gas and stellar masses. The strength of the ALFALFA survey is clearly illustrated here: its high sensitivity allows us to explore the trend over a wide range in H I masses. Observing only the most H I-massive galaxies would lead to the incorrect assumption that H I mass is only very weakly dependent on stellar mass.

3.1 H I and optical completeness

It is important to recall that our galaxy sample is H I flux-limited. The completeness of ALFALFA as a function of H I flux and profile width is discussed in Haynes et al. (2011). Assuming no self-absorption, the total H I flux received from a galaxy depends only on the H I mass, and the luminosity distance to the galaxy, D_L , in Mpc:

$$M_{\text{HI}} = 2.356 \times 10^5 D_L^2 (1+z)^{-1} \int S_\nu d\nu \quad (1)$$

where M_{HI} is in solar masses, and the integral is the total flux in Jy km s^{-1} . The $(1+z)$ factor accounts for the dif-

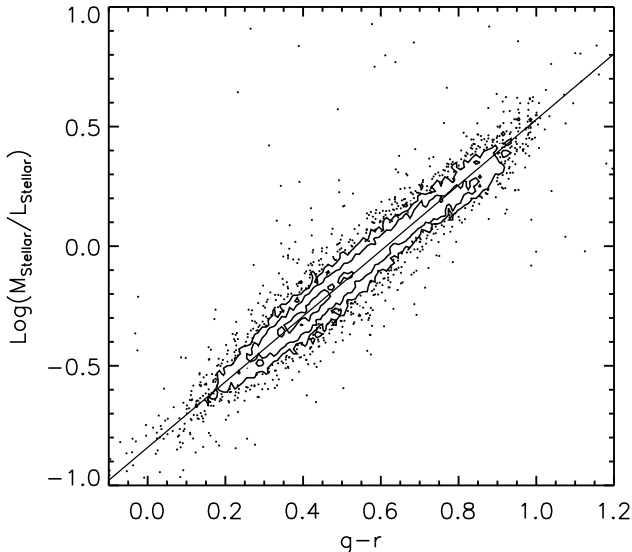


Figure 2. The $\log(M_*/L_{*i})$ vs $(g-r)$ relation derived from the spectroscopic ALFALFA–SDSS galaxies, using M_* from the MPA–JHU catalogue, and L_{*i} from the galaxies’ SDSS i -band apparent magnitudes. The solid black line shows the fit to the data points.

ference between the observed and rest-frame profile width. Due to the distance dependence, galaxies with low M_{HI} are only detected at the lowest redshifts, and not the full survey volume. This completeness leaves the area towards the bottom right of the locus of points in the figure underpopulated, as these galaxies are both relatively gas-poor, and their volume density is low. The horizontal grey dashed line in Fig. 1 indicates the 50 per cent completeness of ALFALFA at $z = 0.06$ for a galaxy with width $W_{50} = 150 \text{ km s}^{-1}$, thus galaxies with masses above this are visible over the full survey volume.

In addition to the H I selection, galaxies must also have an SDSS spectrum to appear in Fig. 1. A galaxy can be without a spectrum either because it is fainter than the spectroscopic limit of $r = 17.77$, or was simply not assigned a fibre by the tiling algorithm. Thus, galaxies without spectra span the full range of stellar masses, but galaxies with spectra almost all have $r \leq 17.77$. At $z = 0.06$, the ALFALFA–SDSS galaxies with $r \sim 17.7$ have stellar masses of $\log(M_*) \sim 9.3$. Above this stellar mass, galaxies are brighter than $r = 17.77$ over the full survey volume.

For the galaxies detected in ALFALFA that do not have spectra, and thus stellar masses from the MPA–JHU catalogue, we can estimate their stellar masses using scaling relations from the observed optical magnitudes. A correlation is seen between $\log(M_*/L_{*i})$ and $(g-r)$ in Bell et al. (2003), where L_{*i} is the stellar luminosity derived from the SDSS i -band magnitude. We assume that the H I-selected galaxies without optical spectra are a subset of the full galaxy sample and follow the same scaling relations.

Using the galaxies in the spectroscopic ALFALFA–SDSS sample with known stellar masses, we derive new coefficients for the $\log(M_*/L_{*i}) - (g-r)$ correlation, which reflect the biased nature of our H I-selected galaxy sample. We find $\log(M_*/L_{*i}) = -0.84 + 1.37(g-r)$ for the points

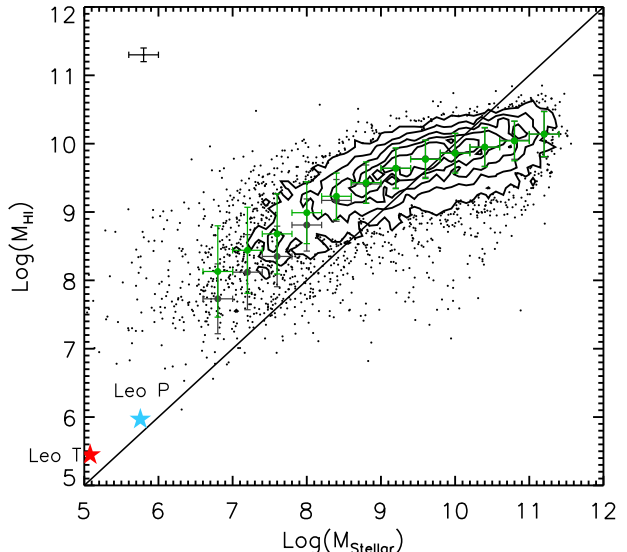


Figure 3. Similar to Fig. 1, but including ALFALFA galaxies that have SDSS imaging but do not have an SDSS spectrum. The stellar masses for these galaxies are computed from the relation derived in Fig. 2. The additional galaxies lessen the severity of, but do not eliminate, the break in the envelope, and the dispersion increases at low masses. The median values for the full sample, from the fourth and fifth columns of Table 1, are shown as green points with error bars, while the median values for the spectroscopic sample are in grey as in Fig. 1. The additional galaxies span the full range of stellar masses.

shown in Fig. 2, and can then estimate the stellar masses for galaxies without spectra using the updated coefficients. The additional points are included in Fig. 3, and lie in the same regions on the $M_{\text{HI}}-M_*$ plane as the galaxies with MPA–JHU stellar masses, thus the shape of the upper envelope is not affected by the optical flux limit.

To populate the top left quadrant of Fig. 1 and Fig. 3, at low stellar mass and high H I mass, galaxies would require $M_{\text{HI}}/M_* \sim 100$. If these galaxies existed in large numbers, they would be sufficiently H I-rich such that ALFALFA would detect them. Their low stellar masses, however, put them near the magnitude limit of the SDSS photometry, $r \sim 22$, which at $z = 0.06$ corresponds to $M_* < 10^7 M_\odot$. There are a small number (less than one per cent of the $\alpha.40$ catalogue) of H I-bright, optically very faint, galaxies within ALFALFA, but they are indeed very rare (Haynes et al. 2011). Thus, the galaxies shown here trace a real upper envelope of H I mass fraction, $f_{\text{HI}} \equiv M_{\text{HI}}/M_*$.

3.2 Models of H I mass vs stellar mass

A number of models exist which incorporate a large range of physical processes for the formation and evolution of galaxies, including accretion, expulsion and ionisation of gas, and conversion of gas into stars. Relevant for this work is the partitioning of gas into neutral, ionized, and molecular components. Modern semi-analytic models are able to match the $z = 0$ stellar and/or H I mass functions, either by construction or as a consistency check. However, none have performed a detailed comparison to the two-dimensional $M_{\text{HI}}-$

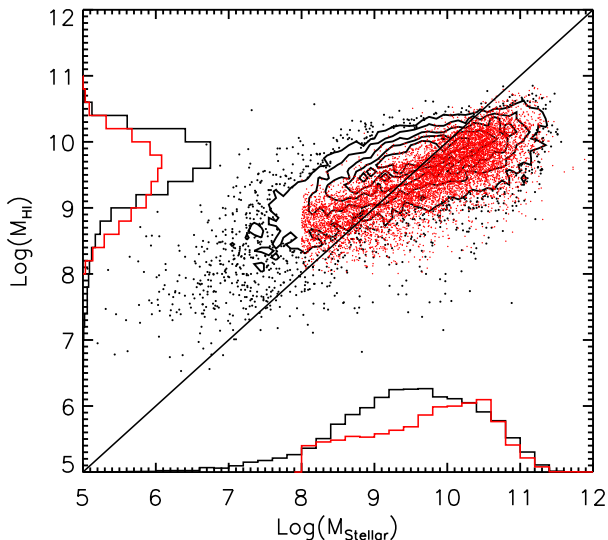


Figure 4. M_{HI} vs M_* for the ALFALFA–SDSS galaxies, including galaxies without spectra (black points and contours), and galaxies extracted from a volume within the S^3 simulations approximating the ALFALFA $\alpha.40$ volume (red points). The S^3 simulated galaxies lack a break in the relation at $M_* \sim 10^9 M_\odot$. The histograms along the x -axis show the stellar mass distributions, and along the y -axis show the HI mass distributions, for the data and simulations in black and red, respectively.

M_* distribution over the full range of galaxy masses shown in Fig. 1. This comparison tests whether the HI gas is located in galaxies of the correct stellar mass.

We have chosen to make a first comparison with galaxies extracted from the SKA Simulated Skies (S^3) simulations² (Obreschkow et al. 2009a, Obreschkow et al. 2009b). The simulations build on the dark matter framework of the Millenium Simulation (Springel et al. 2005) and the semi-analytic galaxy formation prescriptions of De Lucia & Blaizot (2007). Details regarding how M_{HI} is computed for the simulated galaxies can be found in Obreschkow et al. (2009a). The S^3 galaxies are in reasonably good agreement with the HIPASS HI mass function at $M_{\text{HI}} > 10^8 M_\odot$ and the Tully-Fisher relations at $z = 0$.

Fig. 4 compares the ALFALFA–SDSS galaxies (black points and contours) to the S^3 simulated galaxies (red points). The S^3 galaxies are extracted from a simulation volume approximating the ALFALFA $\alpha.40$ volume, also incorporating the 50 per cent completeness limits from Equations 4 and 5 in Haynes et al. (2011). The simulated galaxies are only shown for M_* and $M_{\text{HI}} > 10^8 M_\odot$, as the underlying dark matter simulation does not resolve smaller galaxies. The simulated galaxies overlap with the data at the highest HI and stellar mass, but the locus of points does not follow the ALFALFA–SDSS data traced by the black contours. The difference is largest near the break in the observed galaxy distribution. While the simulations are restricted to $M_{\text{HI}} > 10^8 M_\odot$, there is some evidence that haloes hosting galaxies with $M_* < 4 \times 10^9 M_\odot$ have only existed for a few simulation timesteps, and their properties are not yet

fully converged (Obreschkow et al. 2009a). However, differences between the simulations and data already appear at $M_* = 10^{10} M_\odot$.

The black and red histograms along the x - and y -axis in Fig. 4 show the distributions of stellar and HI masses for the data and simulation, respectively. The simulation has too many high stellar mass ($M_* > 10^{10} M_\odot$) galaxies in the HI -selected sample, and too few galaxies with $10^9 < M_* < 10^{10} M_\odot$. The simulated galaxies with moderate stellar masses ($10^8 < M_* < 10^{10} M_\odot$) are also too HI -poor with respect to the observed data. This suggests that model galaxies of present-day stellar masses around $M_* \sim 10^9 M_\odot$ recently had too little cold gas accretion or star formation efficiency was too high. This, in turn, could indicate missing physics in the model, such as a missing prescription for ram pressure stripping or neglected non-linearities in the partitioning between ionised, atomic and molecular gas.

A further comparison can be made with the smoothed particle N -body + hydrodynamics simulations from Davé et al. (2013). Galaxies extracted from their smaller simulation volume of ~ 45 Mpc on a side with the ‘ezw’ outflow model show qualitatively similar behaviour to the S^3 galaxies, seen as green dots in Fig. 5. Also shown in the figure is the mean trend of M_{HI} as a function of M_* for the galaxy population simulated by Popping, Somerville, & Trager (2014) (blue points with $2\text{-}\sigma$ error bars). These simulations are tuned to match the $z = 0$ stellar mass function, and the only selection criterion imposed here was that the galaxies are disk-dominated, with $M_{\text{bulge}}/M_{\text{total}} < 0.4$ to reflect the bias of the ALFALFA galaxies toward disks. As no restrictions on the observed HI flux is imposed on the galaxy sample extracted, relatively HI -poor galaxies may be biasing the mean M_{HI} toward lower values. Unlike the S^3 model, the simulations and models by Davé et al. (2013) and Popping, Somerville, & Trager (2014) have not yet been turned into mock skies. Therefore, it is currently impossible to extract virtual samples that match the ALFALFA+SDSS selection from these models. Although a hint of a break in the relation is seen from the Popping et al. simulations, it is at $M_* \sim 10^{10} M_\odot$, much higher than seen in the data.

The different behaviour of the galaxies at low and high stellar masses with respect to their HI content is a challenge for simulations. As seen in Fig. 4 and Fig. 5, none of the simulated galaxies reproduce the two regimes, implying a mass-dependent ingredient is missing in the prescriptions regulating the HI fraction in galaxies. In fact, galaxies are not scale-free with respect to their HI fraction. Whether the transition is governed by stellar mass, HI mass or dark matter halo properties is unclear.

4 DISCUSSION

Considering the complexity of the interactions between gas and stars, and the diversity of galactic environments, it is remarkable that a distinct upper envelope of HI mass at a given stellar mass exists at all. One might naively expect that stochastic processes such as environment-dependent gas accretion, different types of outflows, galaxy mergers and subsequent triggered star formation prohibit such a relation. In the following discussion we attempt to explain the upper

² <http://s-cubed.physics.ox.ac.uk/>

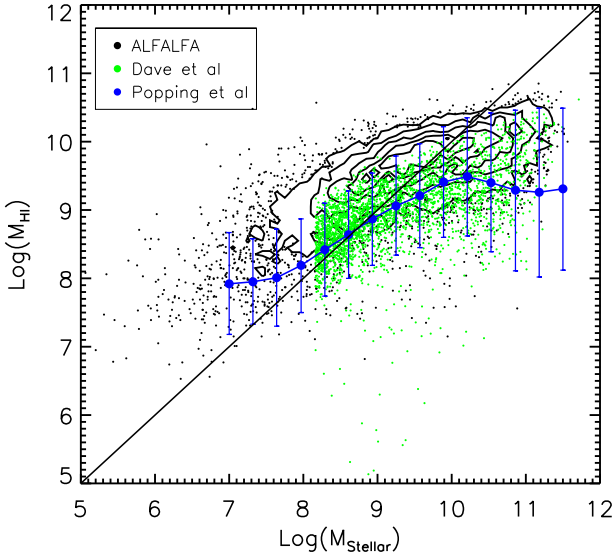


Figure 5. M_{HI} vs M_* for the ALFALFA–SDSS galaxies, including galaxies without spectra (black points and contours), and simulated galaxies from Davé et al. (2013) (green dots) and Popping, Somerville, & Trager (2014) (blue dots with $2\text{-}\sigma$ error bars). The Davé 2013 galaxies follow a similar trend to the S^3 galaxies, while the Popping 2014 simulations do show a break in the relation, albeit at a higher stellar mass than the ALFALFA galaxies.

M_{HI} envelope, and the break in the slope seen in the data at $M_* \sim 10^9 M_\odot$.

The buildup of H I mass and stellar mass is different from other mass relations, such as the correlation between the mass of central black holes and their host spheroids. In the former, stellar mass is built at the expense of the H I reservoir. A major merger of two gas-rich disks results in a triggered burst of star formation, resulting in a massive stellar system with only a fraction of the resulting total mass retained as H I. For the latter mass relation, both the black hole and spheroid can continue to grow, provided there is a source of fuel.

It is important to remember that the objects appearing in the current work are H I-selected, and represent only galaxies with a significant mass of neutral hydrogen. The figures show a snapshot during the phase when they are H I-rich, and does not represent an evolutionary locus for galaxies to follow. Galaxies below the mass sensitivity of the ALFALFA survey galaxy lie below the locus of points.

4.1 What causes the upper limit of f_{HI} ?

From Fig. 1, it is clear that there is a stellar mass-dependent upper limit on galaxies’ H I-to-stellar mass ratio. In the following, we investigate possible causes of this upper limit.

4.1.1 Dark matter halo spin parameter

While discussing the properties of the ALFALFA galaxies, Huang et al. (2012b) make a convincing argument for galaxies with higher H I fractions at a given stellar mass existing in dark matter haloes with larger spin parameters, and thus

have more extended disks (see their Figure 14b). This is consistent with work from Boissier & Prantzos (2000), who find that haloes with large spin parameters host more extended H I disks, along with a more quiescent star formation history. A similar link between halo spin parameter and H I disk size is found in Obreschkow et al. (2009a). Also note that there is a tight positive correlation between the mass of an H I disk and the H I disk radius, as seen in Figure 7 of Verheijen & Sancisi (2001), showing that as disks become more massive, they grow larger. This is a natural consequence of the upper limit on H I density found by Bigiel et al. (2008), for example, beyond which H I rapidly becomes molecular.

Following the method outlined in Huang et al. (2012b), we compute the dark matter halo spin parameters for the ALFALFA–SDSS galaxies. From Boissier & Prantzos (2000), we define the dimensionless halo spin parameter, λ , as:

$$\lambda = \frac{\sqrt{2}V_{\text{rot}}^2 R_d}{GM_{\text{halo}}} \quad (2)$$

where V_{rot} is the rotation velocity of the disk, R_d is the scale length of the stellar disk, assumed to have an exponentially declining surface density, and M_{halo} is the halo mass. Equation 2 is only appropriate for mass distributed in regular disks, which the vast majority of galaxies at the high stellar mass end are. Further, Equation 2 assumes that an equal fraction of mass and specific angular momentum is transferred from the halo to the disk, i.e. $m_{\text{disk}}/j_{\text{disk}} = 1$ (Boissier & Prantzos 2000). We determine the galaxies’ inclination, i , using the r -band axis ratio b/a from the SDSS imaging, and assume an intrinsic axis ratio of $q_0 = 0.2$ for reasons outlined in Huang et al. (2012b):

$$\cos^2 i = \frac{(b/a)^2 - q_0^2}{1 - q_0^2}$$

From this we can convert the H I profile width from the ALFALFA catalogue, W_{50} , into the rotation velocity, V_{rot} , via $V_{\text{rot}} = (W_{50}/2)/\sin(i)$. R_d is extracted from the SDSS database as the r -band exponential fit scale radius, converted to kpc. We convert the V_{rot} to the rotation velocity of the associated dark matter halo, V_{halo} , via the relation found in Papastergis et al. (2011). Finally, the virial mass of the dark matter halo is determined from the relation derived from simulations from Klypin, Trujillo-Gomez, & Primack (2011), where $V_{\text{halo}} = 2.8 \times 10^{-2} (M_{\text{halo}} h)^{0.316}$.

Empirically, we find a positive correlation between H I fraction and halo spin: at any fixed stellar mass $M_* > 10^8 M_\odot$, galaxies with higher H I fractions sit in haloes with higher spin parameters. This finding is consistent with the picture that a high spin can stabilise a large H I disk to prevent it from clumping and forming stars. A natural consequence of this finding is that very high H I mass fractions, or equivalently, very high H I masses at a given stellar mass, would require very high spin parameters. However, theoretically, the spin is limited by the amount of infall and tidal torque haloes can experience during the proto-galactic growth. Explicit numerical N-body simulations of CDM-haloes by Knebe & Power (2008) find an upper limit around $\lambda \sim 0.2$, independent of halo mass. This value is consistent

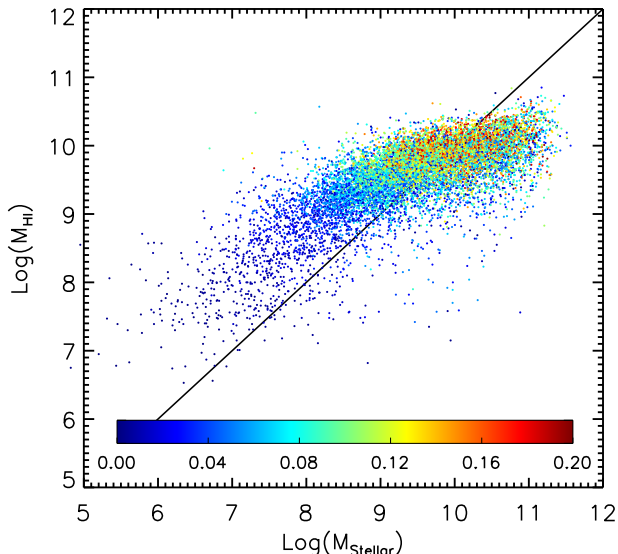


Figure 6. M_{HI} vs M_* for the ALFALFA–SDSS galaxies, including galaxies without spectra, colour coded by their dark matter halo spin parameter. At high masses, galaxies with the larger f_{HI} are also located within haloes with the largest spin parameter. At low masses, all haloes have low spin parameters, even though these galaxies have the highest H I fractions.

with the highest spin parameters measured in this study. Combining the theoretical prediction of an upper limit in the spin parameter with the empirical correlation between spin and H I fraction provides a plausible explanation of the H I fraction in galaxies: The maximum H I fraction is set by the upper limit in the spin parameter.

As H I observations only provide a measure of the neutral gas content, the upper limit on H I mass could also be due to ionization of the neutral gas. Portas et al. (2012) find that the H I density in the THINGS galaxies they studied is too high for the background ionizing field to be responsible for the sharp truncation of H I disks, indicating that the maximum H I mass seen here is not due to increasingly large quantities of ionized gas, but is rather an accurate reflection of an upper limit of the gas content of galaxies. Galaxy interactions, or ram-pressure stripping, are also able to truncate H I disks. However, as H I-rich galaxies are generally found in low-to-moderate density environments (Haynes et al. 2011, Huang et al. 2012b), neither of these effects dominate the H I properties of the galaxies discussed here.

Investigating the dark matter halo spin parameter upper limit, and the formation of large galaxies in haloes with high spin parameter, will help explain the behaviour of the most H I-massive galaxies and the corresponding upper limit on H I mass. At these high stellar masses, the galaxies are regular, massive disks, which are resistant to small perturbations, and star formation can proceed efficiently. The HighMass project (Huang et al. 2014) aims to study in detail the most H I-rich, massive galaxies. Preliminary results for two galaxies from their sample (Hallenbeck et al. 2014) indicate that one, UGC 12506, indeed has a large, extended H I disk and is located in a rapidly spinning dark matter halo, consistent with the general trend found here. The other, UGC 9037, has a more centrally concentrated H I

distribution, with non-circular flows within the disk. Fairly regular optical and H I morphology argues against a recent major merger, rather suggesting accretion from a gaseous halo. Similar analyses of their full sample will illuminate the relative importance of dark matter halo spin properties as compared to environmental or morphological factors for the high mass galaxy population.

4.1.2 Galaxy morphology

At the low stellar mass end ($M_* < 10^9 M_\odot$), the upper envelope is not delimited by high halo spin parameter, even though these galaxies have the largest H I fractions of all the galaxies. Therefore, some other mechanism must restrict the H I fraction. To test whether environmental effects set an upper limit in f_{HI} in these low-mass galaxies, we employ the morphological information derived from the Galaxy Zoo project (Lintott et al. 2008), which can separate the ALFALFA–SDSS galaxies into ‘spirals’, ‘mergers’, or ‘unknown’ morphologies, based on human votes. In practice, it is difficult to distinguish between ‘mergers’ and ‘unknowns’, thus we simply require that the galaxies have low probability of being ‘spirals’, $p_{\text{spiral}} < 0.4$. We refer to the resulting galaxies as irregular. The following is not sensitive to the exact restrictions on the galaxy type percentages.

At stellar masses below $10^9 M_\odot$, the upper envelope of H I fraction is heavily populated by irregular galaxies. As the galaxies are low mass, their morphology is easily disrupted. The number of irregular galaxies then drops significantly between $10^9 M_\odot < M_* < 10^{10} M_\odot$, coinciding with the break in the relation at $M_* \sim 10^9 M_\odot$. The predominance of irregular galaxies at low masses may explain why there is no ordered gradient of halo spin parameters with H I fraction.

The high H I fractions at low stellar mass imply either inefficient star formation in the past, or recent accretion of significant amounts of neutral gas, or a combination of both. Using further information from the MPA–JHU catalogue, we find that the galaxies with the highest H I fractions also have the highest current specific star formation rates of all the ALFALFA galaxies. The metallicity is also lowest for the highest f_{HI} galaxies, dropping below solar values to $12 + \log(\text{O}/\text{H}) < 8$. These two ingredients, coupled with the galaxies’ irregular morphology, favour recent gas accretion. These galaxies could also have recently experienced an interaction with another gas-rich, low mass galaxy. Further H I observations at higher resolution, and deeper optical imaging, would be required to distinguish between the interaction and accretion scenarios.

The link between H I and molecular gas, primarily H_2 , is clearly an important stage in star formation, and in disk galaxies is found to be related to pressure (Blitz & Rosolowsky 2006). For the low-mass galaxies, the lack of massive disks may result in less efficient star formation. Testing this hypothesis requires simulations with sufficient resolution to follow gas accretion onto galaxies with $M_* < 10^{7-8} M_\odot$, coupled with detailed observations of molecular gas of a sample of galaxies.

The transition between the spin-regulated and morphology-regulated regimes, at $M_* \sim 10^9 M_\odot$, also coincides with the transition mass identified within the smoothed particle hydrodynamical simulations of Kereš et al. (2009). They find, at halo masses below

$2 - 3 \times 10^{11} M_{\odot}$, corresponding to baryonic masses of $2 - 3 \times 10^{10} M_{\odot}$, cold accretion is the dominant accretion mode, whereas at masses greater than this, gas accretion switches to hot mode. This is consistent with the low stellar mass galaxies having recently accreted a significant mass of cold gas.

5 SUMMARY

Despite the complicated interactions between galaxies and their environments, along with energetic internal processes, there is a distinct upper limit on the mass fraction of neutral hydrogen a galaxy is able to support. This upper limit argues against the existence of a significant population of the so-called ‘dark galaxies’, which are H I-rich but host very few stars.

The maximum H I fraction is different for low and high stellar mass galaxies, with a break occurring at $M_* \sim 10^9 M_{\odot}$. At high stellar masses, the dark matter halo spin parameter, as well as the H I mass, both reach a maximum. At low stellar masses, the most H I-rich galaxies are morphologically irregular, have low metallicity and current high star formation efficiency, indicating recent gas accretion. The transition between the two mass regimes corresponds to a change in the predominant morphology of the galaxy populations, as well as the transition mass between hot and cold mode accretion in simulations by Kereš et al. (2009) at $M_{\text{baryons}} = 2 - 3 \times 10^{10} M_{\odot}$. Resolved H I observations of the low mass objects will provide further information regarding the H I content and how it is distributed in the galaxies.

ALFALFA, covering several thousands of square degrees with the spectral range and sensitivity to detect galaxies to $z = 0.06$ represents a significant improvement over previous H I studies. The SKA, pathfinder and precursor instruments APERTIF, MeerKAT and ASKAP mark the next advance in H I observations. The most significant gain will be due to the greatly expanded spectral range, which will enable H I in galaxies to be observed to cosmological redshifts. Large numbers of galaxies with $M_{\text{HI}} < 10^9 M_{\odot}$ will be observable at $z \sim 0.4$, populating the low mass end of Fig. 1. The forthcoming H I observations will be supplemented by very deep radio continuum observations, from which dust-free estimates of the star formation can be derived without the need for supplementary optical imaging or spectroscopy. Observing galaxies as a function of their environment and spanning significant lookback time may allow us to view the buildup of the stellar mass from the H I reservoirs.

Combining the next generation of H I surveys with ever improving simulations incorporating more sophisticated gas physics is sure to further our understanding of the buildup of mass within galaxies and how they interact with their environment. The current discrepancies between the observations and simulations, in particular the lack of a break in the envelope of H I mass fraction, indicate physics not yet properly incorporated in the simulations.

ACKNOWLEDGMENTS

The Arecibo Observatory is operated by SRI International under a cooperative agreement with the National Sci-

ence Foundation (AST-1100968), and in alliance with Ana G. Mndez-Universidad Metropolitana, and the Universities Space Research Association. We acknowledge the work of the entire ALFALFA collaboration team in observing, flagging, and extracting the catalogue of galaxies used in this work.

Funding for the SDSS and SDSS-II was provided by the Alfred P. Sloan Foundation, the Participating Institutions, the National Science Foundation, the U.S. Department of Energy, the National Aeronautics and Space Administration, the Japanese Monbukagakusho, the Max Planck Society, and the Higher Education Funding Council for England. The SDSS was managed by the Astrophysical Research Consortium for the Participating Institutions. The SDSS Web Site is <http://www.sdss.org/>.

The SDSS is managed by the Astrophysical Research Consortium for the Participating Institutions. The Participating Institutions are the American Museum of Natural History, Astrophysical Institute Potsdam, University of Basel, University of Cambridge, Case Western Reserve University, University of Chicago, Drexel University, Fermilab, the Institute for Advanced Study, the Japan Participation Group, Johns Hopkins University, the Joint Institute for Nuclear Astrophysics, the Kavli Institute for Particle Astrophysics and Cosmology, the Korean Scientist Group, the Chinese Academy of Sciences (LAMOST), Los Alamos National Laboratory, the Max-Planck-Institute for Astronomy (MPIA), the Max-Planck-Institute for Astrophysics (MPA), New Mexico State University, Ohio State University, University of Pittsburgh, University of Portsmouth, Princeton University, the United States Naval Observatory, and the University of Washington.

NM wishes to acknowledge the South African SKA Project for funding the postdoctoral fellowship position at the University of Cape Town. KMH’s research has been supported by the South African Research Chairs Initiative (SARChI) of the Department of Science and Technology (DST), the Square Kilometre Array South Africa (SKA SA), and the National Research Foundation (NRF). We are grateful to Gergő Popping and Mika Rafieferantsoa for providing H I and stellar masses from their simulations. This work has benefitted from many useful discussions with a number of people, including, but not limited to, Jacqueline van Gorkom, Martha Haynes, Gyula Jozsa, Andrew Pontzen, Eric Wilcots, and Ian Heywood. We thank the anonymous referee for helpful comments and quick response which improved this paper. This research has made use of NASA’s Astrophysics Data System.

REFERENCES

- Abazajian K. N., et al., 2009, *ApJS*, 182, 543
- Baldry I. K., Glazebrook K., Brinkmann J., Ivezić Ž., Lupton R. H., Nichol R. C., Szalay A. S., 2004, *ApJ*, 600, 681
- Barnes D. G., et al., 2001, *MNRAS*, 322, 486
- Bell E. F., McIntosh D. H., Katz N., Weinberg M. D., 2003, *ApJS*, 149, 289
- Bigieli F., Leroy A., Walter F., Brinks E., de Blok W. J. G., Madore B., Thornley M. D., 2008, *AJ*, 136, 2846
- Bigieli F., Blitz L., 2012, *ApJ*, 756, 183

- Blitz L., Rosolowsky E., 2006, *ApJ*, 650, 933
- Boissier S., Prantzos N., 2000, *MNRAS*, 312, 398
- Brinchmann J., Charlot S., White S. D. M., Tremonti C., Kauffmann G., Heckman T., Brinkmann J., 2004, *MNRAS*, 351, 1151
- Bruzual G., Charlot S., 2003, *MNRAS*, 344, 1000
- Carilli C. L., Rawlings S., 2004, *NewAR*, 48, 979
- Davé R., Katz N., Oppenheimer B. D., Kollmeier J. A., Weinberg D. H., 2013, *MNRAS*, 434, 2645
- De Lucia G., Blaizot J., 2007, *MNRAS*, 375, 2
- Giovanelli R., et al., 2005, *AJ*, 130, 2598
- Hallenbeck G., et al., 2014, *arXiv*, arXiv:1407.1744
- Haynes M. P., et al., 2011, *AJ*, 142, 170
- Huang S., Haynes M. P., Giovanelli R., Brinchmann J., Stierwalt S., Neff S. G., 2012a, *AJ*, 143, 133
- Huang S., Haynes M. P., Giovanelli R., Brinchmann J., 2012b, *ApJ*, 756, 113
- Huang S., et al., 2014, *ApJ*, 793, 40
- Johnston S., et al., 2008, *ExA*, 22, 151
- Jonas J. L., 2009, *IEEEP*, 97, 1522
- Kauffmann G., et al., 2003b, *MNRAS*, 341, 33
- Kennicutt R. C., Jr., 1998, *ApJ*, 498, 541
- Kereš D., Katz N., Fardal M., Davé R., Weinberg D. H., 2009, *MNRAS*, 395, 160
- Klypin A. A., Trujillo-Gomez S., Primack J., 2011, *ApJ*, 740, 102
- Knebe A., Power C., 2008, *ApJ*, 678, 621
- Lagos C. D. P., Lacey C. G., Baugh C. M., Bower R. G., Benson A. J., 2011, *MNRAS*, 416, 1566
- Le Fèvre O., et al., 2005, *A&A*, 439, 845
- Leroy A. K., Walter F., Brinks E., Bigiel F., de Blok W. J. G., Madore B., Thornley M. D., 2008, *AJ*, 136, 2782
- Lintott C. J., et al., 2008, *MNRAS*, 389, 1179
- Meyer M. J., et al., 2004, *MNRAS*, 350, 1195
- Obreschkow D., Croton D., De Lucia G., Khochfar S., Rawlings S., 2009a, *ApJ*, 698, 1467
- Obreschkow D., Klöckner H.-R., Heywood I., Levrier F., Rawlings S., 2009b, *ApJ*, 703, 1890
- Papastergis E., Martin A. M., Giovanelli R., Haynes M. P., 2011, *ApJ*, 739, 38
- Popping G., Caputi K. I., Somerville R. S., Trager S. C., 2012, *MNRAS*, 425, 2386
- Popping G., Somerville R. S., Trager S. C., 2014, *MNRAS*, 442, 2398
- Portas A., Brinks E., Usero A., Walter F., de Blok W. J. G., Kennicutt R. C., 2012, *EAS*, 56, 129
- Serra P., et al., 2012, *MNRAS*, 422, 1835
- Springel V., et al., 2005, *Natur*, 435, 629
- Tremonti C. A., et al., 2004, *ApJ*, 613, 898
- Verheijen M. A. W., Sancisi R., 2001, *A&A*, 370, 765
- Verheijen M. A. W., Oosterloo T. A., van Cappellen W. A., Bakker L., Ivashina M. V., van der Hulst J. M., 2008, *AIPC*, 1035, 265
- Walter F., Brinks E., de Blok W. J. G., Bigiel F., Kennicutt R. C., Jr., Thornley M. D., Leroy A., 2008, *AJ*, 136, 2563
- York D. G., et al., 2000, *AJ*, 120, 1579